# Gas Detector Developments in AMS: Vertical position, total energy, and Bragg detector

*Jackson T. H.* Dowie[1,*], *L. Keith* Fifield[1], *Stefan* Pavetich[1], and *Stephen G.* Tims[1]

[1]Department of Nuclear Physics and Accelerator Applications, The Australian National University, Canberra 2601

**Abstract.** Gas ionisation chamber detectors are the workhorses of Accelerator Mass Spectrometry (AMS), providing essential isobar suppression and ion identification. Continued developments in detector resolution, performance, and reliability directly translate into improved AMS sensitivity and precision. In this contribution we report three recent developments in the gas detectors used at the Australian National University (ANU). First, we demonstrate a cathode-based vertical position measurement in the Flexible Anti-Scatter Multi-Anode (FASMA) detector, achieving a vertical position resolution of 1.71 mm (FWHM) and using this information to diagnose and correct incomplete charge collection onto the first anode. Second, we implement an independent total-energy measurement based on the grid signal in the single-grid, multi-anode FASMA detector, obtaining an energy resolution of 2.1% (FWHM), improved relative to 2.8% from the conventional anode-sum signal. Third, we describe the design of a new Bragg detector under construction at ANU and discuss analogue and digital analysis techniques for ion identification. Commissioning of the Bragg detector is expected in early 2026. These detector developments are expected to lead to enhanced isobar discrimination and measurement accuracy in future AMS campaigns at ANU.

## 1 Introduction

Gas ionisation chambers are the standard detection systems for heavy-ion Accelerator Mass Spectrometry (AMS) [1]. Their ability to tolerate high count rates, insensitivity to radiation damage, and flexibility make them superior to solid-state detectors for the measurement of heavy ions, in addition to their capability for ion identification and isobar suppression. Improvements in detector functionality directly translate to higher precision and lower detection limits.

Gas ionisation chamber detectors collect the charge deposited in the detector gas by ionisation from the ion traversing the detector volume [1]. A transverse electric field transports the liberated charge from the ion track to the electrodes. The movement of the ionisation charge induces current on the electrodes of the detector which is presented as a voltage signal from charge-sensitive preamplifiers. This basic design is illustrated in figure 1. Typical detectors gasses include propane and isobutane.

In a multi-anode gas-ionisation chamber detector, the anode plane is segmented along the beam direction. The electric field between the anodes and the cathode defines the collection region for each anode. The liberated electrons are collected by the anodes for each section of track thereby measuring the energy lost by the ion in each portion of its track. This allows for ion identification as different ion species have different energy deposition curves in the gas.

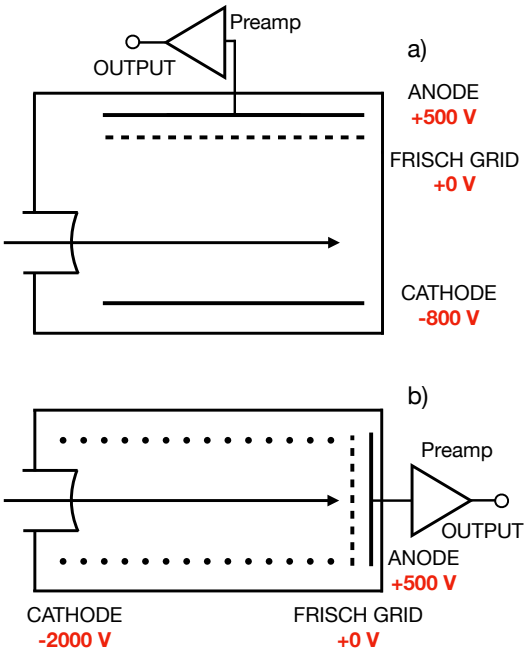


Figure 1: Schematic diagram of a typical gas ionisation chamber detector (a) and of a typical Bragg detector (b). An energetic ion enters from the left (arrow), travelling through a window (typically Mylar) and the detector gas (typically propane or isobutane). The electric field is perpendicular to the ion track for the standard gas ionisation chamber detector (a) and parallel to the ion track for the Bragg detector (b).

*e-mail: jackson.dowie@anu.edu.au

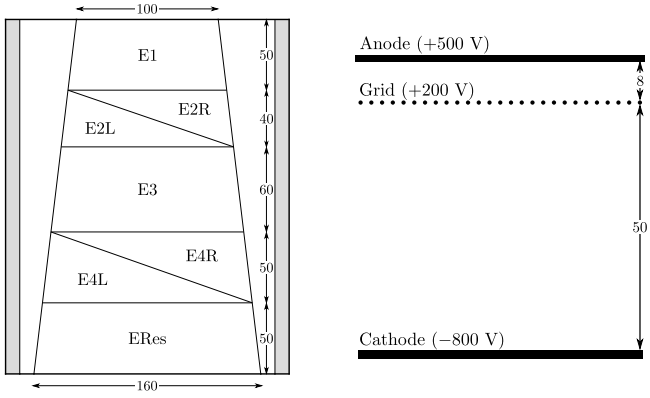


Figure 2: Schematic diagram of the FASMA detector. (Left) Horizontal plane, with segmented anode configuration, beam entry from top. (Right) Vertical plane with segmented anode, single Frisch grid and cathode. Dimensions are in millimetres. The tapered design and lateral buffer spaces provide protection from field distortions close to the detector wall and highly scattered events. From reference [3].

The Flexible Anti-Scatter Multi-Anode detector is one such type of detector in use at the ANU [2, 3]. It is a 5-anode ionisation chamber detector with two of the electrodes split diagonally for position measurements. A schematic illustration of the FASMA detector is shown in figure 2. It is presently optimised for the discrimination of $^{53}$Mn from $^{53}$Cr but is also used for $^{60}$Fe, $^{26}$Al and $^{10}$Be measurements at the ANU [4]. It has been designed for the easy replacement of the anode board allowing for optimisation for any given ion-pair. Although the detector possesses horizontal position sensitivity, it currently lacks vertical position sensitivity.

An alternative, complementary approach is the use of a Bragg detector [5]. In this concept, the electric field is oriented parallel to the ion track and the induced current on the readout electrode is a time-projected image of the energy-loss curve, integrated through the charge-sensitive pre-amplifier. An illustrative schematic of a Bragg detector is shown in figure 1. Bragg detectors have been successfully implemented at several AMS facilities and can demonstrate excellent ion discrimination [6, 7].

This paper reports three detector developments at the ANU. First, we explore the use of the FASMA cathode signal to measure the vertical position (entry close or far from the cathode) of the ion track in the detector, and we quantify the resulting position resolution. Second, we develop an independent total energy measure derived from the FASMA Frisch-grid signal, despite the detector employing only a single, un-shielded Frisch grid. Third, we present the design of a new Bragg detector for AMS at ANU and comment on analogue and digital analysis techniques for ion determination from the Bragg detector output. Together, these developments extend the capabilities of the existing FASMA detector and report on the construction of next-generation instrumentation for AMS at ANU.

## 2 Exploration of vertical position in FASMA

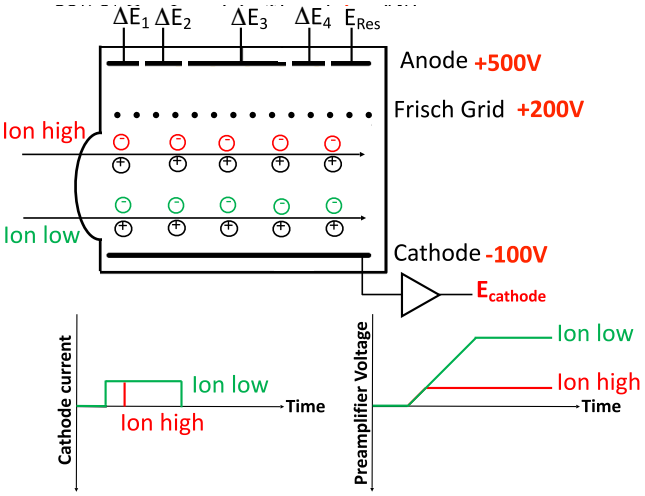


Figure 3: Schematic illustration of how the cathode signal describes the vertical position of the ion track. A low entry, green, induces significantly more current on the cathode than a high entry (red), resulting in a larger pre-amplifier output signal.

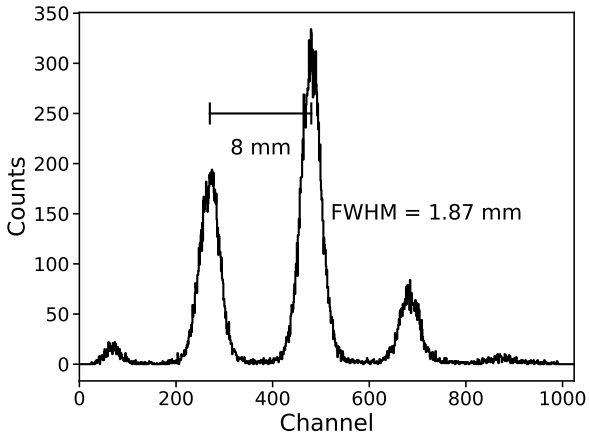


Figure 4: Plot of vertical position resolution of the FASMA detector. The FWHM resolution of 1.87 mm shown is the true detector response convoluted with the 1 mm wide entrance slit. The deconvolved, true resolution is 1.71 mm.

The FASMA detector has horizontal position sensitivity but currently lacks vertical position sensitivity. It is possible, however, to derive a vertical position signal from the cathode. This is shown in figure 3. Variations in the height of the ion track relative to the cathode translate into a height-dependent voltage signal from the pre-amplifier. The cathode signal is produced by the induced current from the movement of the liberated electrons in the gas. In principle the positive ions created move within the electric field between the electrodes as well. However they are orders of magnitude slower and can be considered stationary for these considerations. For ions entering high in the

detector, i.e. far from the cathode and close to the Frisch grid, the cathode is exposed to the moving electrons for only a short time before the charge moves past the Frisch grid and is shielded from the cathode, producing a small signal. For a low entry, the cathode is exposed to the moving charge for a longer time, producing a larger signal.

The sensitivity of the FASMA detector to vertical position was tested in the ANU gas-filled magnet (GFM) with 105 MeV $^{37}$Cl ions. A mask with five 55 mm by 1 mm horizontal slots separated vertically by 8 mm defined five vertical positions spanning the 40 mm height of the detector's entrance window. The ions are spread out both vertically and horizontally by the 4 Torr of nitrogen gas in the GFM. Figure 4 shows the measurement results. The resulting observations can be made:

1. The signals from the different slots are well separated. The width of the central peak (1.84 mm FWHM) corresponds to a true vertical resolution of 1.71 mm after deconvolving with the 1 mm width of the slot.

2. For the first time, the extent of vertical scattering by the gas in the GFM is visible, and provides reassurance that essentially all of the ions are collected by the 40 mm high window.

3. The detector is not centred vertically. Subsequently, a discrepancy in the vertical positioning of the detector was discovered. This has now been corrected.

Historically, the signal from the first anode electrode (E1) has been of limited utility due to a pronounced low-energy tail. Now that vertical position information is available, it was discovered that this tail arises from incomplete charge collection when the ions enter either high or low into the detector. In the former case, some electrons were being collected by the frame of the Frisch grid. In the latter, some electrons were being collected by the window. We have redesigned the window frame so that it extends further into the detector, and have shortened the cathode so that electric field lines no longer terminate on the window. Notwithstanding these modifications, any residual effect of the vertical position on E1 can be compensated using the vertical position information. Hence, the E1 signal now makes an additional useful contribution to the discrimination against isobaric interferences.

## 3 Independent total energy measurement for FASMA

The FASMA detector consists of a cathode, an undivided Frisch grid, and a divided anode plane [2, 3], as shown in figure 2. Under standard operation, the role of the Frisch grid is to shield the anode from the rest of the detector volume, ensuring the anode signals are independent of the position of the ion track on entry. The measurement of the total ion energy can be performed by having a single anode, by having two Frisch grids and taking the total energy signal from the shielded, second Frisch grid, or by summing all anodes in a multi-anode detector. In the case of the

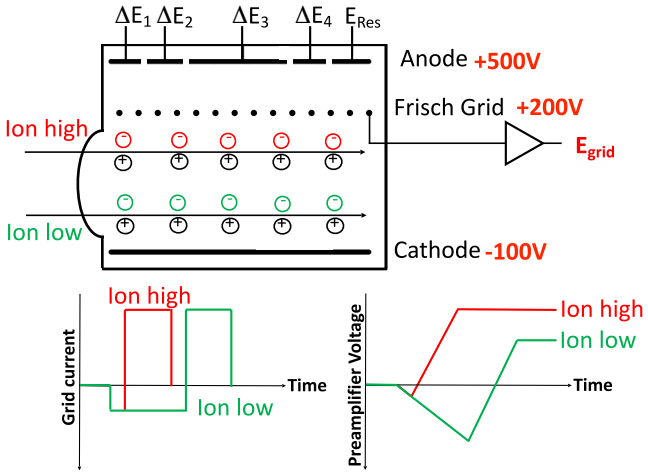


Figure 5: Schematic illustration of how to extract the total deposited energy of the ion from the output of an unshielded Frisch grid. The initial component of the signal varies with vertical position but the second component - after the charge drifts past the Frisch grid - is invariant to the initial track position and depends solely on the total deposited energy. This positive component of pre-amplifier signal can be extracted by differentiation, e.g. a timing filter amplifier or digital system.

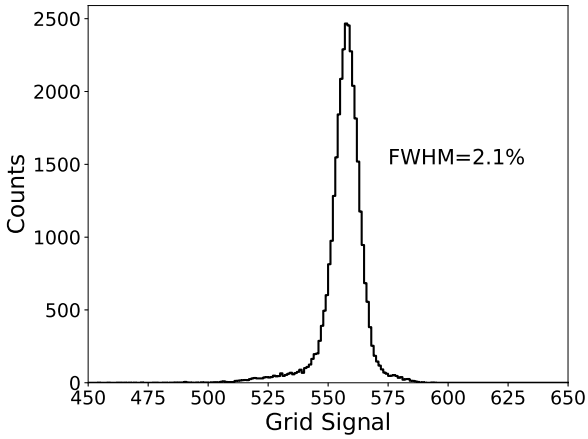


Figure 6: The total energy signal recorded from the single Frisch grid in the FASMA detector. An energy resolution of 2.1% (FWHM) was obtained, superior to the summed anode resolution of 2.8%.

FASMA detector, the total energy must be determined by summing the respective anode signals but due to noise and variable gain, this results in a decrease of the resolution. The question: is there a way to perform an independent measure of the total energy for a one-grid, divided-anode detector such as FASMA?

Our approach is illustrated in figure 5. The key fact is that the signal developed by the electrons moving from the Frisch grid to the anode only depends on the total charge (proportional to ion energy) irrespective of the entry height of the ion. This is because the distance from Frisch grid to the anode is a constant 8 mm. This is shown in figure 5

where the second, positive component of the developed pre-amplifier signal is independent of the entry height of the ion.

A charge-sensitive pre-amplifier is used to produce a signal from the grid. This integrates the current, producing the outputs shown in figure 5. Clearly, this output is not position insensitive and cannot be used to derive the total energy directly. To solve this problem, we have used a timing filter amplifier to differentiate the pre-amplifier output signal, re-obtaining the pulse shape from figure 5.

Since electron drift velocities at these field strengths in isobutane are ≈40 mm/$\mu$s, and the grid-anode distance is 8 mm, the duration of the grid–anode pulse in figure 5 is only ≈0.2 $\mu$s. Thus a short differentiation time constant of 0.1 $\mu$s was used.

Figure 6 shows the pulse-height distribution of the timing filter amplifier output. A well-defined peak representing the total energy of the ions is indeed obtained. The energy resolution of 2.1% is superior to the 2.8% obtained by summing the anode signals. It may be possible to improve the resolution further by digitising the waveform from the pre-amplifier and differentiating it electronically.

## 4 Development of new Bragg Detector

A Bragg detector similar to those in references [6, 7] is under construction for use at ANU as a flexible final detector for heavy-ion AMS. The intent is to extract more information from the deposited ion track resulting in superior ion discrimination and enable us to push both the discovery and precision frontiers in AMS at the ANU.

Figure 7 shows a photograph of the unmounted detector. It consists of 19 gold-plated, hollow discs connected by a resistor chain which defines a constant electric field along the axis, a Frisch grid, and an anode readout plane, all 10 mm apart, for a total length of 210 mm. The aperture of 32 mm and ring spacing of 10 mm ensure that the electric field is uniform to within 1% out to a distance of at least 25 mm from the axis. A divided anode can be used to obtain position information of the track.

Commissioning measurements are planned for early 2026. We plan to start with 104 MeV $^{36}$Cl and $^{36}$S ions in ≈100 mbar of propane as the detector gas so that we can make a direct comparison with the 5-anode ionisation chamber that is normally used for $^{36}$Cl measurements [8, 9]. A 700 nm Mylar detector entrance window will be used and a negative voltage of 2000 V will be applied to the uppermost ring to provide a uniform electric field of 10 V/mm along the axis. Electron drift velocities at this field and gas pressure are approximately 40 mm/$\mu$s. From this starting point, the operating conditions will be explored to optimise the response of the detector. As examples, the Bragg curves for $^{36}$Cl and $^{36}$S and the corresponding Bragg-detector pre-amplifier signals are simulated with SRIM [10] in figure 8.

We plan to test first the standard analogue approach of using two amplifiers with short (0.5–1.0 $\mu$s) and long (≈10 $\mu$s) shaping times. Signals with long shaping time will be used to derive the total energy whereas those with short shaping time provide information on the relative heights of the Bragg peaks. The longer term goal is, however, to develop a digital acquisition system to collect and analyse digitised traces from the pre-amplifier in order to effectively map out the energy-loss distributions shown in figure 8. Analysis algorithms would then be developed to use the additional information for enhanced ion discrimination.

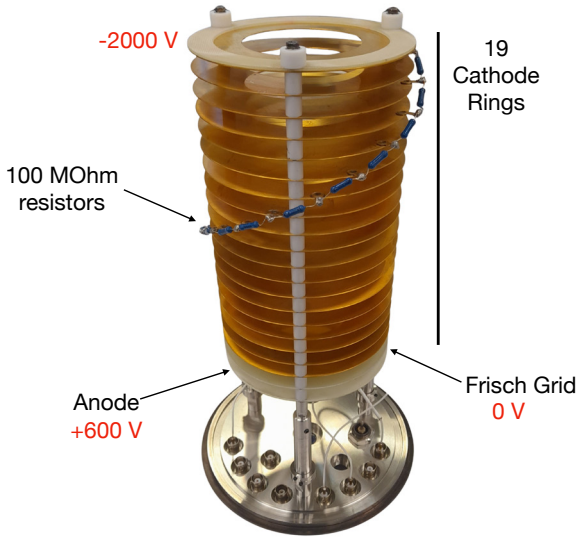


Figure 7: Photo of the unmounted Bragg detector. From the top, there are 19 cathode rings, separated by 100 MΩ resistors, 1 Frisch grid, and 1 anode, all 10 mm apart, for a total length of 210 mm. The anode and Frisch grid have their own voltage connections. The inner bore radius is 32 mm and the outer radius is 60 mm.

## 5 Conclusion

Gas ionisation chambers are central to heavy-ion AMS because they provide robust and flexible detectors capable of ion identification and isobar suppression. In this contribution we have described three recent developments regarding gas detectors at the ANU.

First, we have demonstrated that the cathode signal in the FASMA detector can be used as a precise measure of the vertical position of the ion track. The masked measurement yielded a deconvoluted, vertical resolution of 1.71 mm (FWHM). The resulting position information was used to identify a strong dependence of the first-anode response on entry height which was traced to partial charge interception by the Frisch-grid frame (high entry) and window (low entry). A redesigned entrance-window frame and shortened cathode have eliminated this effect resulting in a usable first-anode signal, adding vertical position and the first-anode signal to the FASMA detector output.

Second, we have implemented a position-independent total energy measurement based on the grid signal in the single-grid FASMA detector. By appropriately shaping the grid pre-amplifier waveform, energy resolution was improved by 25% from 2.8% to 2.1% by using the grid signal instead of the sum signal from all the anodes. We

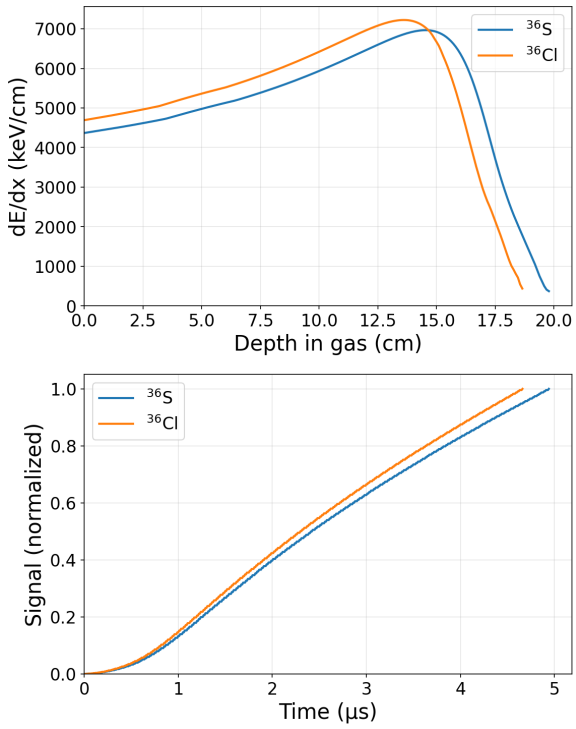


Figure 8: Simulated ion tracks of $^{36}$S and $^{36}$Cl in the Bragg detector (above) and the corresponding pre-amplifier output traces (below). The differences in the energy deposition with depth are apparent in the ion tracks (above) and this produces significantly different pre-amplifier output traces (below). The ion tracks were simulated in SRIM, using 104 MeV $^{36}$S and $^{36}$Cl ions, in 100 mbar propane and with a 700 nm Mylar detector entrance window. The pre-amplifier signals were then calculated a drift velocity of 40 mm/$\mu$s at a 10 V/mm electric field.

expect this to enhance our ion separation, especially in use with the gas-filled magnet, and we are investigating digital acquisition to further improve the resolution.

Third, we have outlined the design and planned analysis strategies for a new Bragg detector for AMS at ANU. The detector will provide a time-resolved measurement of the Bragg curve, enabling both the traditional analogue pulse-shape analysis based on varying shaping times and the modern digital waveform analysis extracting total energy, range, and other shape parameters. Commissioning measurements are planned for 2026.

Taken together, these developments significantly extend the capabilities of the ANU gas detectors for AMS. The additional measurement channels and improved resolutions will contribute directly to better isobar discrimination, lower backgrounds, and enhanced precision in future AMS applications.

## Acknowledgment

The authors acknowledge the facilities, and the scientific and technical assistance provided by Heavy Ion Accelerators (HIA). HIA is supported by the Australian Government through the National Collaborative Research Infrastructure Strategy (NCRIS) program.

## References

[1] L.K. Fifield, *The Methodology and Physics of Accelerator Mass Spectrometry: A Handbook for Students and Practitioners* (ANU, 2025). https://doi.org/10.25911/XQGG-JH37

[2] M. Martschini, L.K. Fifield, M.B. Froehlich, G. Leckenby, S. Pavetich, S.G. Tims, B. Tranter, A. Wallner, New and upgraded ionization chambers for AMS at the Australian National University. Nucl. Instrum. Methods Phys. Res. B **438**, 141–147 (2019). https://doi.org/10.1016/j.nimb.2018.05.039

[3] G. Leckenby, *Remodelling a multi-anode ionisation chamber detector for accelerator mass spectrometry of $^{53}$Mn*. (Honours Thesis, Australian National University, 2017). http://hdl.handle.net/1885/142833

[4] A. Wallner, L.K. Fifield, M.B. Froehlich, D. Koll, G. Leckenby, M. Martschini, S. Pavetich, S.G. Tims, D. Schumann, Z. Slavkovská, Accelerator mass spectrometry with ANU's 14 million volt accelerator. Nucl. Instrum. Methods Phys. Res. B **534**, 48–53 (2023). https://doi.org/10.1016/j.nimb.2022.10.021

[5] C.R. Gruhn, M. Binimi, R. Legrain, R. Loveman, W. Pang, M. Roach, D.K. Scott, A. Shotter, T.J. Symons, J. Wouters, M. Zisman, R. Devries, Y.C. Peng, W. Sondheim, Bragg curve spectroscopy. Nucl. Instrum. Methods **196**, 33–40 (1982). https://doi.org/10.1016/0029-554X(82)90612-7

[6] G.M. Santos, J.C. Acquadro, P.R.S. Gomes, R.M. Anjos, R. Liguori Neto, N. Added, N.H. Medina, N. Carlin, M.M. Coimbra, M.L. di Tada, R.G. Cresswell, L.K. Fifield, The Brazilian Bragg curve detector built for AMS studies. Nucl. Instrum. Methods Phys. Res. B **172**, 310–315 (2000). https://doi.org/10.1016/S0168-583X(00)00374-8

[7] A.M. Müller, M. Döbeli, M. Seiler, H.-A. Synal, A simple Bragg detector design for AMS and IBA applications. Nucl. Instrum. Methods Phys. Res. B **356**, 81–87 (2015). https://doi.org/10.1016/j.nimb.2015.04.056

[8] L.K. Fifield, S.G. Tims, T. Fujioka, W.T. Hoo, S.E. Everett, Accelerator mass spectrometry with the 14UD accelerator at the Australian National University. Nucl. Instrum. Methods Phys. Res. B **268**, 858–862 (2010). https://doi.org/10.1016/j.nimb.2009.10.049

[9] L.K. Fifield, S.G. Tims, J.O. Stone, D.C. Argento, M. De Cesare, Ultra-sensitive measurements of $^{36}$Cl and $^{236}$U at the Australian National University. Nucl. Instrum. Methods Phys. Res. B **294**, 126–131 (2013). https://doi.org/10.1016/j.nimb.2012.04.028

[10] J.F. Ziegler, M.D. Ziegler, J.P. Biersack, SRIM – The stopping and range of ions in matter. Nucl. Instrum. Methods Phys. Res. B **268**, 1818–1823 (2010). https://doi.org/10.1016/j.nimb.2010.02.091